PCCP

Accepted Manuscript

ROYAL SOCIETY OF CHEMISTRY

www.rsc.org/pccp

Journal Name

ARTICLE TYPE

Cite this: DOI: 10.1039/xxxxxxxxxx

Potentiometric and electrokinetic signatures of iron (II) interactions with (α,γ)-Fe_2O_3

Diana Toczydłowska,[a] Karolina Kędra-Królik,*[a] Krzysztof Nejbert,[b] Tajana Preočanin,[c] Kevin M. Rosso,[d] and Piotr Zarzycki*[a]

Received Date
Accepted Date

DOI: 10.1039/xxxxxxxxxx

www.rsc.org/journalname

The electrochemical signatures of Fe(II) interactions with iron (III) oxides is poorly understood, despite its importance in controlling the amount of mobilized iron. Here, we report the potentiometric titration of α,γ-Fe_2O_3 oxides exposed to Fe(II) ions. We monitored *in situ* surface and ζ potentials, the ratio of mobilized ferric to ferrous, and periodically analyzed nanoparticle crystal structure using X-ray diffraction. Electrokinetic potential reveals weak but still noticeable specific sorption of Fe(II) to oxide surface at acidic conditions, and pronounced adsorption at alkaline conditions that results in a surface potential reversal. By monitoring aqueous iron (II/III) fraction, we found that addition of Fe(II) ions produces platinum electrode response consistent with the iron solubility-activity curve. Although, XRD analysis showed no evidence of γ-Fe_2O_3 transformations along the titration pathway despite iron cycling between aqueous and solid reservoirs, the magnetite formation cannot be ruled out.

1 Introduction

Iron (III) oxides are the most widespread transition metal oxides at the Earth's near surface.[1] They are composed of ferric ions, predominantly in an octahedral coordination, which are arranged in close-packed arrays by sharing FeO_6-octahedral edges, faces or corners,[1] thus forming several polymorphic iron oxide forms. These forms inter-convert easily, with goethite and hematite being frequent end-products in natural settings.[1] The majority of these transformations occur via the reductive-dissolution/oxidative-precipitation pathway[1], which is catalyzed by reducing and/or complexing agents. In particular, the dissolution enhancement of iron(III) oxide upon addition of iron (II) ions as a participating reducing agent is a fascinating phenomenon (see ref.[2–5]). Because Fe(II) is a product, the majority of reductive iron (III) oxide transformations occur in the presence of Fe(II) and the redox interaction is autocatalytic. Sorption of Fe(II) is an important step, that possibly governs the overall kinetics of such a mineral transformation. Therefore understanding Fe(II) sorption on and interactions with Fe(III)-oxide surfaces is crucial to elucidating the natural dynamics of Fe-oxide minerals.

For decades, researchers have investigated macroscopic factors that affect Fe(III)-oxide reductive dissolution autocatalyzed by addition of Fe(II) ions (e.g., composition, temperature, exposure to light, particle size, porosity).[1,6–13] Unfortunately, very little is known about the relevant elementary processes at the microscopic level. For instance, we still do not understand how surface electrostatics affect Fe(II) sorption, and how Fe(II) interactions with the oxide surface manifest electrochemical signatures. The main obstacle has been the lack of studies in which pH-dependent surface/diffuse potentials and concentrations of dissolved iron ions and their valance are monitored simultaneously. These quantities are typically recorded in separate measurements and their interdependence rarely confronted.

Here, we report potentiometric titration of a novel electrochemical cell composed of two end-member Fe(III)-oxides. A single-crystal hematite (α-Fe_3O_3) electrode (predominantly (001) crystal face exposed) is immersed in a suspension of maghemite (γ-Fe_2O_3) nanoparticles. The cell represents electrochemical contact between two different crystal structures of identical composition and valence. We have purposely combined two Fe_2O_3 reservoirs to simultaneously monitor the surface (crystal face) and diffuse (nanoparticle) potentials, and also to more realistically mimic environmental conditions, where typically multiple phases coexist.

Both iron oxide reservoirs are studied with and without Fe(II) ions in solution. The ratio of the mobilized Fe(III) to soluble Fe(II) pools is monitored by a platinum electrode similar to previous studies.[14,15] What is more, we periodically examined the ζ-potential and crystal structure of the suspended nanoparticles.

In this report we asked how the ratio of dissolved iron ions is

[a] *Institute of Physical Chemistry, 44/52 Kasprzaka, Warsaw, Poland. Fax: +48 22 343 3333; Tel: +48 22 343 3258; E-mail: kkedrakrolik@ichf.edu.pl, or zarzycki.piotrek@gmail.com*
[b] *Department of Geology, Warsaw University, Warsaw, Poland.*
[c] *Department of Chemistry, University of Zagreb, Zagreb, Croatia.*
[d] *Pacific Northwest National Laboratory, Richland, WA.*

correlated to the surface and diffuse layer potential of α,γ-Fe_2O_3 oxides and whether potential measurements are able to detect Fe(II) sorption and reactive interactions with the oxide surface. The findings shed new light onto mechanisms governing reductive transformation of iron minerals in environment.

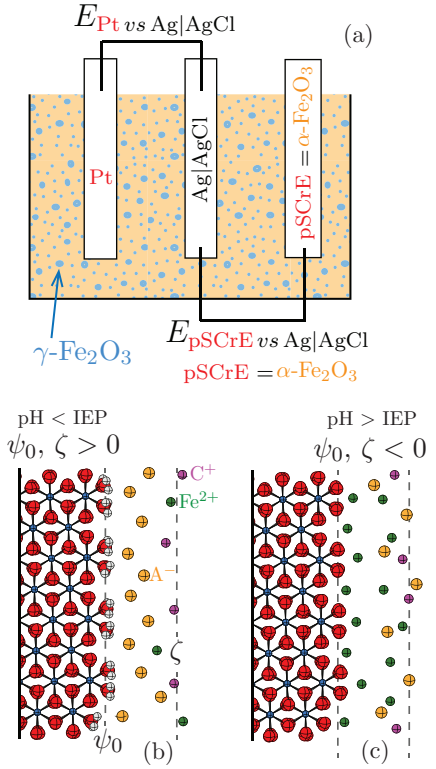

Fig. 1 Electrochemical cell containing suspended γ-Fe_2O_3 nanoparticles, α-Fe_2O_3 single crystal electrode (SCrE), platinum redox electrode (Pt), reference electrode (AgCl|Ag) combined with the glass electrode (pH-meter) (Panel a). The diagram of the charge distribution at the iron(III) oxide/electrolyte interface at pH < IEP (a) and at p H > IEP (b). The background electrolyte ions are denoted by C^+ and A^-.

2 Materials and protocols

Materials. Maghemite (γ-Fe_2O_3) nanoparticles ($\varnothing < 50$ nm) and ferrous chloride (purity 98%) were purchased from Sigma Aldrich. Other chemicals were of an analytical reagent grade. A natural hematite crystal obtained from Cada de Pedramine, Congonhas do Campo, Minais Gerais, Brazil was used in constructing the single-crystal electrode, of which a visually determined (001) face was exposure selected for the exposed surface of the electrode.

Apparatus. The ζ-potential was measured by ZetaPlus Zeta Potential Analyzer (Brookhaven Instruments Corporation, US). The alkalimetric titration was performed by using the 665 Dosimat (Metrohm, US) assisted with/without the ultrasound mixing to avoid particle aggregation. The electrodes relative potentials were measured in a three electrode setup (Fig. 1a), which was composed of single-crystal hematite electrode (SCrE),[18–22] platinum electrode and the combined reference (Ag|AgCl)/glass electrode (Metrohm, US).

Reagents preparation. All solutions were prepared using the distilled and deionized water. We used two suspension stocks (i,ii) containing the maghemite nanoparticles (1 g/dm^3) suspended in electrolyte solution of i) NaCl (0.001 mol/dm^3), HCl (0.001 mol/dm^3) and ii) $NaNO_3$ (0.001 mol/dm^3), HNO_3 (0.001 mol/dm^3). We added maghemite particles to freshly prepared electrolyte solution at pH=3, as pH value changed due to the oxide protonation, we brought it back to pH=3 by adding HCl.

Measurements. To avoid oxidation due to prolonged exposure to air, all measurements were carried out under argon atmosphere using degassed, freshly prepared suspensions. During the titration experiment, a small fraction of cell solution (1 ml) was collected for separate ζ-potential measurements in $\Delta\psi_0$=20 mV intervals in the glass-electrode indication. Argon was pumped through the cell to remove the dissolved oxygen and carbon dioxide down to minimal content. Alkalimetric titration was carried out from pH 3 to 9, by addition of titrant (100 μL of 0.1 mol/dm^3 NaOH) as only the glass-electrode potential stabilizes. The stability of pH-meter was indicated by constant voltage value over 5 minutes (by constant value we mean that only voltage fluctuations bellow the threshold of 1 mV were allowed). In other words, the titration interval was not fixed, but adjusted in fly based on the pH-stabilization (titration interval increases as oxide surface gains more charge).

Powder X-ray diffraction (XRD) analysis of nanoparticles before and after extracted from the reaction zone during titration was carried out using a PHILIPS X'PERT PRO diffractometer working in Bragg-Brentano reflection geometry. The samples were mounted on a standard metal holder, and irradiated with CoKa radiation with the wavelength $\lambda = 1.789$ Å (i.e., longer then the K-adsorption edge of iron: $\lambda_{\mathrm{Fe}} = 1.743$ Å). Samples have been irradiated for 8 hrs. Data were collected over 2θ range from 4.0 to 89.9° using PIXcel detector working in 1D mode (allowing to simultaneously counts in about $\delta(2\theta)$= 3.35° range by using 255 active channels). The beam acceleration voltage and current intensity were equal to 40 keV and 30 mA, respectively. The phases were initially identified by the HighScore Plus software, and latter re-examined by the CrystalDiffract program.

3 Methodology

Electrokinetic potential. The ζ-potential measurement of the maghemite nanoparticles suspension provides insight into the electrostatic potential at the shear plane, which is geometrically defined as the region at the boundary between the stagnant structure of accumulated counter-ions (Helmholtz planes) and the mobile co- and counter-ions in the diffuse part of electrical double layer.

The key descriptor of the ζ-potential curve is the pH value at which ζ=0, the so-called isoelectric point (IEP, $\mathrm{pH_{IEP}}$). Although the reported $\mathrm{pH_{IEP}}$ values for natural and synthetic Fe_2O_3 are very scattered (between 4 and 8, see ref.[23]), maghemite is generally considered to be more acidic (lower $\mathrm{pH_{IEP}}$) than hematite.

Platinum electrode potential. In our setup, the platinum electrode is sensitive only to mobilized ferric-ferrous ions ratio (i.e., $E \sim \ln\left[Fe^{3+}\right]/\left[Fe^{2+}\right]$).[14,15] In other words, it acts as an electron

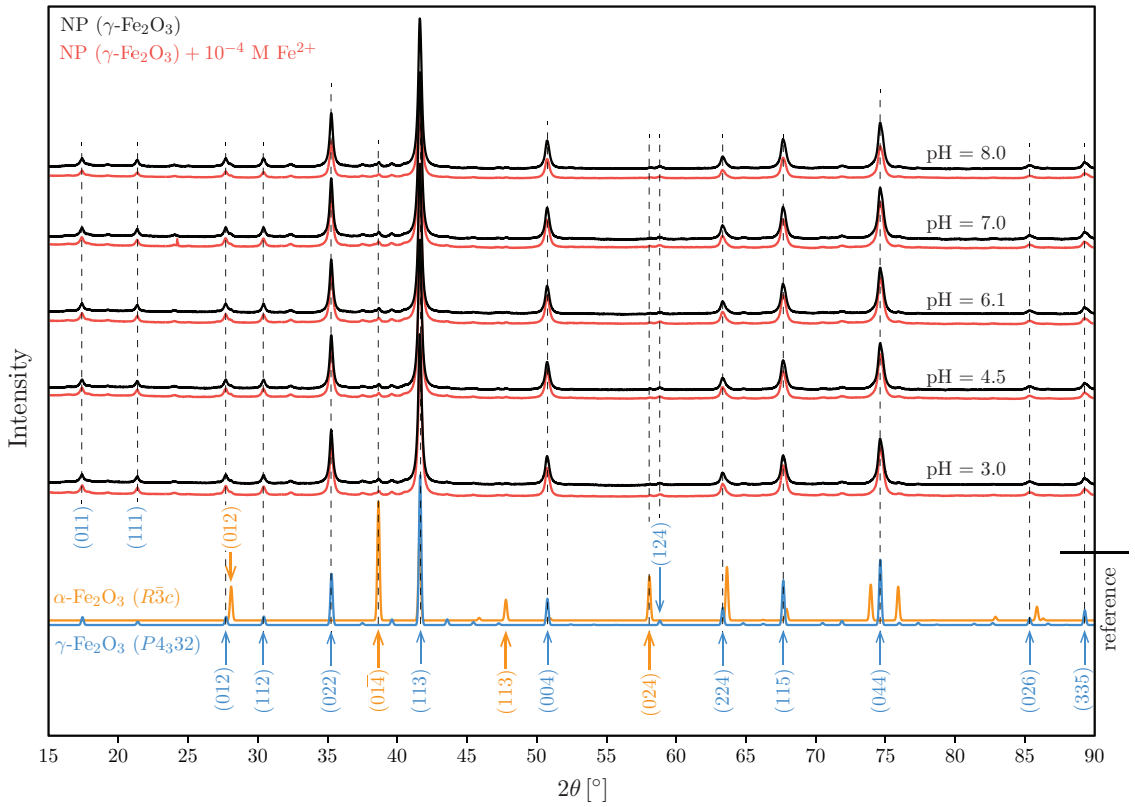

Fig. 2 Powder X-ray diffractograms of the γ-Fe_2O_3 particles extracted from the cell at varying pH values in the presence (red lines) and absence (black lines) of the Fe(II) ions. XRD spectra were obtained at $\lambda = 1.789$ Å (Co lamp). The simulated XRD spectra (blue/orange lines at the bottom) were obtained using CrystalDiffract software package, by using the hematite structure (α-Fe_2O_3, $R\bar{3}c$, $a = b = 5.038, c = 13.772, \alpha = \beta = 90°, \gamma = 120°$) reported by Blake *et al.*[16] and by maghemite structure (γ-Fe_2O_3, $P4_332$, $a = b = c = 8.347, \alpha = \beta = \gamma = 90°$) reported by Shmakov *et al.*[17]

source or sink only for the Fe(III)/Fe(II) redox couple.

Single-crystal hematite electrode. Single-crystal hematite (SCrE) electrodes are routinely used in many research groups to assess the unique electrochemical behavior of the isolated mineral faces.[18–21,24–26] The natural hematite crystal was fixed in the plexiglass holder, the surface was cleaned with ethanol and deionised water. The resistance of electrode surface was around 5×10^8 Ω. We used the SCrE potential measurement to monitor the surface potential response to detachment, complexation and reduction of the surface iron sites. In this work we restrained from converting SCrE potential to the surface potential,[18–20,27] therefore the reported values are relative ones.

4 Results and Discussion

α/γ-Fe_2O_3 surfaces. Hematite is considered the most stable ferric oxide (end-form of many iron oxide transformations),[1,10,11] therefore it is less prone to dissolve than maghemite (dissolution rate of γ-Fe_2O_3 is of an order of magnitude larger than of α-Fe_2O_3 see ref.[28]). For this reason, one can expect that most of the mobilized iron comes from the induced dissolution of γ-Fe_2O_3 nanoparticles. However, there are also reports of spontaneous α-Fe_2O_3 to γ-Fe_2O_3 transformation as the particle size decreases, which is due to lower surface energy of the maghemite structure[29] (i.e., $\Delta G_s(\alpha\text{-}Fe_2O_3)/\Delta G_s(\gamma\text{-}Fe_2O_3) \sim 2.5$ see ref.[11]). For this reason, we used maghemite nanoparticles instead of hematite ones to avoid possible phase transformation during titration. We also periodically monitored the crystal structure (XRD) of the nanoparticles during titration experiments.

γ-Fe_2O_3 structure. The XRD analysis confirmed that the nanoparicles are almost pure γ-Fe_2O_3, and the hematite content is within the range of 4-8% as indicated by a diagnostic reflection at 2θ=38.6° (hematite (01$\bar{4}$) face; Fig. 2). The crystal structure remains unchanged during titration, even if Fe(II) ions are added (Fig. 2), however because of the structural similarities between maghemite and magnetite (Fe_3O_4), the transition from maghmetite to magnetite may remain undetected, and it cannot be ruled out based on the X-ray diffraction analysis.

Effect of electrolyte. It has been suggested that some anions can adsorb specifically to the oxide surface promoting oxide dissolution by weakening Fe-O bonds. For instance, Sidhu *et al.*[28] observed that the Cl^- ions increase the proton-promoted dissolution of iron oxides as compared to a more inert effect of ClO_4^- ions. Such specific interactions manifest typically by a shift in isoelectric point as a function of electrolyte concentration and anion type.

In our study, we observed that the isoelectric point (pH_{IEP}) of the nanopartricle suspension is equal to 6.1 for two types of background electrolyte (NaCl and $NaNO_3$, see Fig. 3) and remains insensitive to electrolyte concentration. Interestingly, similar values were reported for hematite nanoparticles (pH_{IEP})[30] and for the (001) hematite SCrE (pH_{PZC}).[19,31]

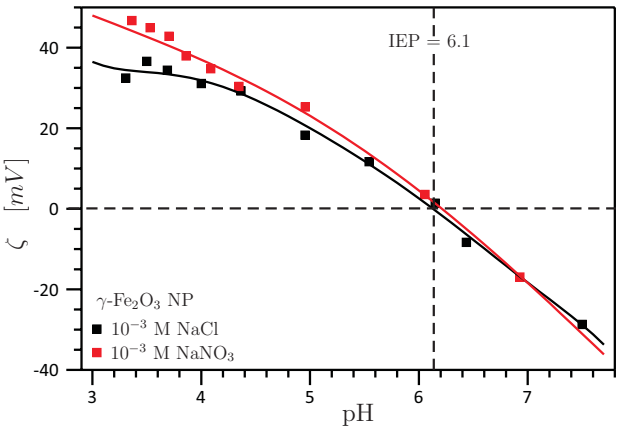

Fig. 3 Effect of electrolyte type on the electrokinetic potential.

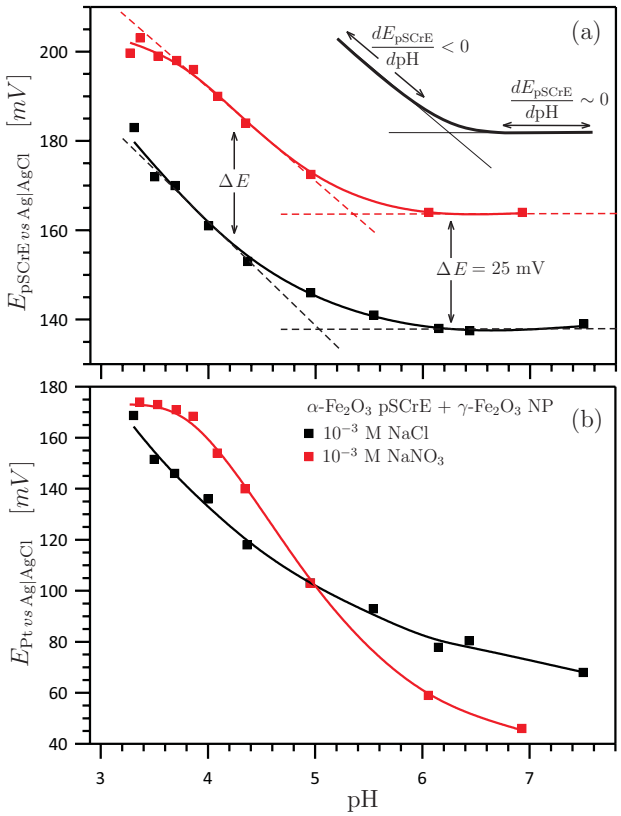

Fig. 4 Effect of electrolyte type on hematite electrode relative potential (a) and platinum electrode potential (b) in the presence of maghemite nanoparticles.

The hematite SCrE potential decays exponentially with increasing pH until it reaches a plateau at pH > pH_{IEP} (Fig. 4a). Similar inert behavior above pH_{PZC} was reported for the hematite (001) SCrE electrode by others.[31–34] The plateau appearance manifests in the pH range where the oxide surface becomes inert, presumably due to termination predominantly by doubly coordinated Fe_2OH groups[19,32].

Anion accumulation in the Helmholtz planes seems to be larger for chloride than for nitrite ions (see $\Delta E = 25$, Fig. 4a), but the potential shift is only on the order of the thermal energy (k_BT (T=298K) = 25.7 mV), thus prediction of any sorption preference is rather inconclusive.

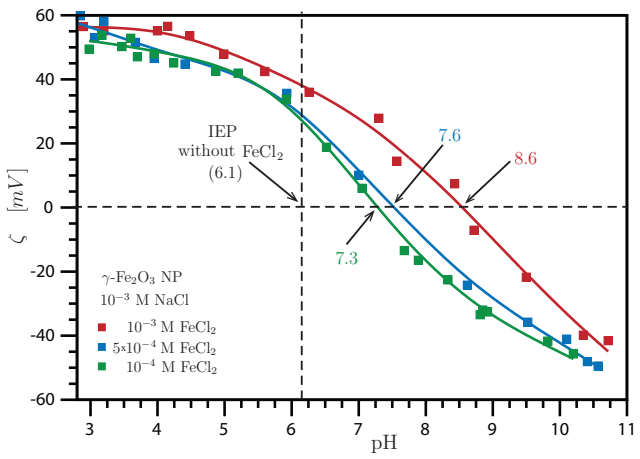

Fig. 5 Effect of addition Fe(II) ions on the electrokinetic potential.

In almost all cases reported here, the platinum electrode potential decays with increasing pH value (Figure 4b). This decay is an indication of the decreasing Fe^{3+}/Fe^{2+} ratio. As shown in Fig. 4, $E_{Pt}=f(pH)$ has an s-shape with an inflection point around pH 5 in the case of $NaNO_3$ or it has an exponential decay resembling $E_{SCrE}=f(pH)$ in the case of NaCl electrolyte.

Iron (II) ions. It is generally accepted that the presence of Fe(II) affects significantly iron oxide electrostatics[35,36]. The absolute value of electrokinetic potential shifts towards more alkaline pH with increasing concentration of Fe(II) ions.[35,36] An increase in ζ-potential in the acidic region with increasing concentration of Fe(II) indicates specific adsorption of iron (II) to the iron oxide despite repulsive electrostatic interactions with the positively charged surface.[35] Indeed, we observe the shift in IEP value towards more alkaline values (from 6.1 to 7.3-8.6, Fig. 5), with typically larger values of ζ at a given pH value than reported for pure electrolyte (i.e., without Fe(II) ions, Fig. 3).

A similar increase in the IEP and sometimes even a more dramatic charge-reversal behavior have been observed previously for mono- di- and trivalent cations sorbed at the metal oxide surface.[37–39] Indeed, in the alkaline pH region potentials recorded by the hematite and platinum electrodes exhibit the reverse pH-dependence by showing a surprising increase with increasing pH (Fig. 6). Because, ζ-potential curves do not exhibit the charge reversal character, we conclude that Fe(II) ions accumulate close to the the oxide surface (in the rigid Helmholtz plane) rather than in the diffuse layer.

In other words, the recorded hematite and platinum potential profiles (Fig. 6) posses a semi-parabolic shape with a minimum near the nanoparticle IEP. The increase in the Fe(III) ions concentration results in the increase of the platinum electrode potential.[14,15] An analogous increase in the hematite potential is probably caused by the additional protonation of newly created surface groups upon surface Fe detachment.

We find it also remarkable that the electrode potentials measured in the presence of Fe(II) ions (Fig. 6) bear some resemblance to the pH-dependent activity plot of Fe(III) ions. In our opinion, this is a manifestation that the surface chemistry of the

oxide in the presence of Fe(II) and iron ion redox-recombination at the platinum surface are both governed by the ferrous-ferric electrochemical balance in the aqueous phase.

The hematite electrode response is affected by the addition of γ-Fe_2O_3 nanoparticles only in the narrow pH range pH $\in (3.5;6.2)$ (E_{SCrE} increases by ~ 5 mV, see Fig. 6a). In contrast, the platinum potential is significantly affected by the presence of nanoparticles, but only at pH < 4 (ΔE_{Pt} =140 mV at pH=3.1, Fig. 6b). The fact that nanoparticles affect the electrode potential only at low pH is quite surprising, and it may be due to the increased dissolved Fe(III) pool, which is stable only in the acidic environment.

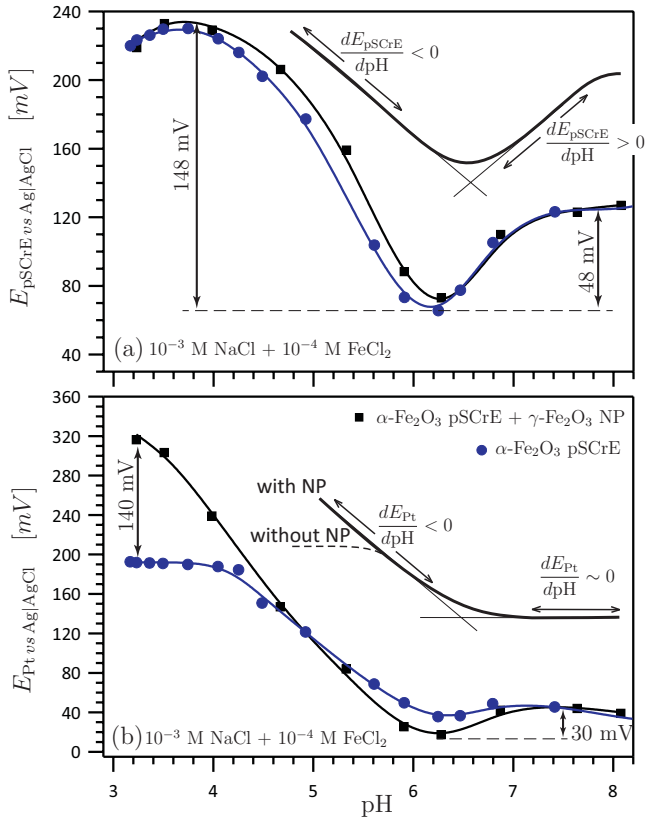

Fig. 6 Effect of the maghemite nanoparticles on the potential difference recorded by the polycrystalline hematite electrode (a) and platinum electrode (b) in the presence of the dissolution enhancing ferrous ions.

5 Conclusions

In this work, we reported that the presence of Fe(II) ions strongly affects the electrochemical response of α,γ-Fe_2O_3 in potentiometric titration experiments.

We found that the pH_{IEP}(γ-Fe_2O_3) value is identical for NaCl and $NaNO_3$ electrolytes, which suggests that simple ions accumulate only due to nonspecific electrostatic attraction. In contrast, ferrous ions adsorb specifically on the oxide surfaces shifting pH_{IEP} values appreciably (towards more alkaline values).

In most cases, we observed the plateau in hematite surface potential at pH $>$ pH_{IEP}, supporting the prevalent believe in the inert character of the (001) crystal face.[19,32] However, if Fe(II) ions are added in excess, we observe an inversion in hematite potential around pH_{IEP}, producing a pH-dependence similar to the iron(III) solubility curve and other studies of specific multivalent cation accumulation.[39]

The platinum electrode potential plays a role of an Fe(III)/Fe(II) ratio probe, which shows that the amount of ferric ions in solution decreases with increasing pH. These results indicate that the iron speciation near the oxide and platinum electrodes is strongly coupled to the solution phase, and an imbalance of mobilized Fe(III)/Fe(II) at one interface is quickly propagated to the other.

We believe that the platinum electrode introduces the energetically most favorable pathway for mobilized iron to equilibrate, and for this reason we have not observed any significant structural or morphological changes in the nanoparticles. Although we did not detect any crystallographic changes in nanoparticles, some more subtle and difficult to detect transitions cannot be ruled out such as magnetite formation, particularly at higher pH. This allowed us to focus predominantly on the surface electrochemistry of α,γ-Fe_2O_3 surfaces without complications due to uncontrollable oxide transformations. Therefore, introduction of the platinum electron source/sink (platinum) for Fe(II/III) mobilized ions is convenient in studying electrochemistry of iron oxides, especially less stable ones.

We concluded that electrochemical equilibrium between mobilized aqueous iron ions appears to be a driving force for redox-reactivity of iron(III) oxides, whereas specific and electrostatic interactions govern Fe(II) sorption to the charged oxide surface.

Acknowledgement

This work was supported by Ministry of Science and Higher Education (MNiSW grant IP2012 059872). D. T. thanks Department of Chemistry, University of Zagreb, Croatia and T. P. for hospitality during D. T. summer internship sponsored by MNiSW grant IP2012 059872. K. M. R. was supported by the Geosciences Research Program in the U.S. Department of Energy, Office of Basic Energy Sciences, Division of Chemical Sciences, Geosciences & Biosciences (Pacific Northwest National Laboratory, Richland WA). We thank Odeta Qafoku from Pacific Northwest National Laboratory (Richland, WA) for insightful discussion of XRD experimental data.

References

1 U. S. Rochelle M Cornell, *The Iron Oxides*, Wiley-VCH, Weinheim, 2nd edn., 2003.

2 C. A. Gorski and M. M. Scherer, in *C. A. Gorski and M. M. Scherer*, American Chemical Society, Washington, DC, 2011, pp. 315–343.

3 C. A. Gorski, R. M. Handler, B. L. Beard, T. Pasakarnis, C. M. Johnson and M. M. Scherer, *Environ. Sci. Technol.*, 2012, **46**, 12399–12407.

4 P. Zarzycki, D. M. Smith and K. M. Rosso, *J. Chem. Theory Comput.*, 2015, **11**, 1715–1724.

5 P. Zarzycki, S. Kerisit and K. M. Rosso, *J. Phys. Chem. C*, 2015, **119**, 3111–3123.

6 M. F. Hochella, S. K. Lower, P. A. Maurice, R. L. Penn, N. Sa-

hai, D. L. Sparks and B. S. Twining, *Science*, 2008, **319**, 1631–1635.
7 D. M. Cwiertny, G. J. Hunter, J. M. Pettibone, M. M. Scherer and V. H. Grassian, *J. Phys. Chem. C*, 2009, **113**, 2175–2186.
8 C. A. Lanzl, J. Baltrusaitis and D. M. Cwiertny, *Langmuir*, 2012, **28**, 15797–15808.
9 G. Rubasinghege, R. W. Lentz, M. M. Scherer and V. H. Grassian, *Proc. Natl. Acad. Sci. U. S. A.*, 2010, **107**, 6628–6633.
10 A. Navrotsky, L. Mazeina and J. Majzlan, *Science*, 2008, **319**, 1635–1638.
11 A. Navrotsky, C. Ma, K. Lilova and N. Birkner, *Science*, 2010, **330**, 199–201.
12 A. S. Madden and M. F. Hochella, Jr., *Geochim. Cosmochim. Acta*, 2005, **69**, 389–398.
13 T. Echigo, D. M. Aruguete, M. Murayama and M. F. Hochella, Jr., *Geochim. Cosmochim. Acta*, 2012, **90**, 149–162.
14 E. Silvester, L. Charlet, C. Tournassat, A. Géhin, J.-M. Greneche and E. Liger, *Geochim. Cosmochim. Acta*, 2005, **69**, 4801–4815.
15 Z. Shi, J. T. N and P. G. Tratnyek, *Environ. Sci. Technol.*, 2011, **45**, 1586–1592.
16 R. L. Blake, R. E. Hessevick, T. Zoltai and L. W. Finger, *Am. Mineral.*, 1966, **51**, 123–129.
17 A. N. Shmakov, G. N. Kryukova, S. V. Tsybulya, A. L. Chuvilin and Solovyeva, L.P., *J. Appl. Crystallogr.*, 1995, **28**, 141–145.
18 S. Chatman, P. Zarzycki and K. M. Rosso, *Phys. Chem. Chem. Phys.*, 2013, **15**, 13911.
19 P. Zarzycki, S. Chatman, T. Preočanin and K. M. Rosso, *Langmuir*, 2011, **27**, 7986–7990.
20 T. Preočanin and N. Kallay, *Surf. Eng.*, 2008, **24**, 253–258.
21 S. Chatman, P. Zarzycki, T. Preočanin and K. M. Rosso, *J. Colloid Interface Sci.*, 2013, **391**, 125–134.
22 T. Preočanin, A. Čop and N. Kallay, *J. Colloid Interface Sci.*, 2006, **299**, 772–776.
23 M. Kosmulski, *J. Colloid Interface Sci.*, 2011, **353**, 1–15.
24 S. Chatman, P. Zarzycki and K. M. Rosso, *ACS Appl. Mater. Interfaces*, 2015, **7**, 1550–1559.
25 K. Shimizu and J. F. Boily, *J. Phys. Chem. C*, 2015, **119**, 5988–5994.
26 K. Shimizu and J. F. Boily, *Langmuir*, 2014, **30**, 9591–9598.
27 P. Zarzycki and T. Preočanin, *J. Colloid Interface Sci.*, 2012, **370**, 139–143.
28 P. S. Sidhu, R. J. Gilkes, R. M. Cornell, A. M. Posner and J. P. Quirk, *Clays Clay Miner.*, 1981, **29**, 269–276.
29 I. V. Chernyshova, M. F. Hochella, Jr and A. S. Madden, *Phys. Chem. Chem. Phys.*, 2007, **9**, 1736.
30 N. Kallay, T. Preočanin, J. Marković and D. Kovačević, *Colloids Surf., A*, 2007, **306**, 40–48.
31 T. Preočanin, Ž. Majić, D. Kovačević and N. Kallay, *Adsorpt. Sci. Technol.*, 2007, **25**, 429–437.
32 J.-F. Boily, S. Chatman and K. M. Rosso, *Geochim. Cosmochim. Acta*, 2011, **75**, 4113–4124.
33 J. Lützenkirchen, F. Heberling, F. Supljika, T. Preočanin, N. Kallay, F. Johann, L. Weisser and P. J. Eng, *Farad. Discuss.*, 2015, **180**, 55–79.
34 J. Lützenkirchen, T. Preočanin, F. Stipić, F. Heberling, J. Rosenqvist and N. Kallay, *Geochim. Cosmochim. Acta*, 2013, **120**, 479–486.
35 Z.-X. Sun, F.-W. Su, W. Forsling and P.-O. Samskog, *J. Colloid Interface Sci.*, 1998, **197**, 151–159.
36 C. J. Serna and M. P. Morales, in *Surface and Colloid Science*, ed. E. Matijević and M. Borkovec, Kluwer Academic / Plenum Publishers, New York, 2004, pp. 27–81.
37 M. Siebentritt, P. Volovitch, K. Ogle and G. Lefèvre, *Colloids Surf., A*, 2014, **440**, 197–201.
38 C. Schneider, M. Hanisch, B. Wedel, A. Jusufi and M. Ballauff, *J. Colloid Interface Sci.*, 2011, **358**, 62–67.
39 N. Lee, D. A. Sverjensky and R. M. Hazen, *Environ. Sci. Technol.*, 2014, **48**, 9358–9365.